Supplementary Information for
Revealing the electronic structure of a carbon nanotube carrying a supercurrent

by J.-D. Pillet, C. H. L. Quay, P. Morfin, C. Bena, A. Levy Yeyati and P. Joyez

Sample fabrication

Carbon nanotubes were grown by chemical vapor deposition from catalyst grains deposited on a 1 µm SiO_2 insulating layer atop a highly doped Si substrate used as a back gate. As measured with an atomic force microscope, the tubes have diameters of 1-3 nm and are thus expected to be single-walled carbon nanotubes (SWNT). The SWNTs are then located with respect to gold alignment marks using Scanning Electron Microscopy (SEM) and electron-beam lithography of a MAA-PMMA bilayer is used to form a suspended mask through which we deposit the electrodes. The electrodes consist of 3 nm Ti/100 nm Al for the loop and 1 nm Ti/40 nm Al for the tunnel probe; they are deposited through the suspended mask at different angles in a single pump-down. The loop, which is well-connected to the CNT was deposited first after 2 hours of heating at 110°C in a vacuum of $\sim 10^{-7}$mb followed by rapid quenching down to -80°C. Evaporation is started when the temperature is around 0°C. The tunnel contact is then evaporated at another angle. This process yields quite frequently contact resistances measured at room temperature of $15 - 25\,\mathrm{k}\Omega$ and $\sim 100\,\mathrm{k}\Omega$ respectively which depend weakly on back gate voltage. Room temperature conductance measurements between two well-connected electrodes on either side of such tunnel probes indicate that the latter does not cut the tube. After lift-off, the sample was wire-bonded and cooled down in a dilution refrigerator equiped with carefully filtered lines.

Measurements

The differential conductance of the tunnel probe was measured using standard lock-in techniques at frequencies $\sim 200\,\mathrm{Hz}$ and an ac excitation of 2 µV. All electrical lines are shielded and filtered and we use a room temperature amplifier with a low back action on the tunnel contact to ensure a low electronic temperature. In previous experiments a very similar setup was shown to have a tunneling spectroscopy resolution of $\sim 15\,\mu\mathrm{eV}$ [1].

Extracting the Density of States (DOS) from the differential conductance

Assuming thermal equilibrium and energy-independent transmission between the probe and the tube, the tunnel current is expressed as

$$I(V) \propto \int \left(n_{TP}(\epsilon - \mathrm{eV}) - n_{NT}(\epsilon)\right) \rho_{NT}(\epsilon)\rho_{TP}(\epsilon - \mathrm{eV})d\epsilon$$

where n_i are Fermi functions and ρ_i are DOSs, with NT (TP) standing for Nanotube (Tunnel probe). In the present experiment, the tunnel probe is superconducting. We assume that its DOS is nearly BCS, with a phenomenological Dynes "depairing" imaginary part $i\gamma\Delta$ added to the energy, to smooth out the BCS singularity (here γ is a dimensionless parameter) [2]:

$$\rho_{TP}(\epsilon) = \mathrm{Re}\frac{|\epsilon|}{\sqrt{(\epsilon + i\gamma\Delta)^2 - \Delta^2}}$$

The differential conductance can be expressed as a convolution product ($\otimes$)

$$\frac{\partial I}{\partial V}(V) \propto \left(g \otimes \rho_{NT}\right)(eV) = \int g(eV - \epsilon, V)\rho_{NT}(\epsilon)d\epsilon$$

of the unknown tube DOS ρ_{NT} with the fixed function

$$g(E, V) = \left(n_{NT}(E - eV) - n_{TP}(E)\right)\rho'_{TP}(E) - n'_{TP}(E)\rho_{TP}(E),$$

with respect to E.

Since convolution is a linear operation, its implementation on a discretized set of data $\left[\frac{\partial I}{\partial V}\right]$ can be expressed as a matrix operation :

$$\left[\frac{\partial I}{\partial V}\right] \propto M_g.\left[\rho_{NT}\right]$$

where M_g is a matrix appropriately sampling g over its two variables. We obtain the least-square error estimate of the DOS in the nanotube by left-multiplying the latter equation by the Moore-Penrose pseudo-inverse [3] of M_g. The differential conductance can thus be deconvolved to get ρ_{NT} simply by multiplying it by a fixed matrix. We have checked that edge effects due to the finite measurement range are negligible. The adjustable parameters in this deconvolution process are the probe gap Δ, the depairing amplitude γ, and the temperature. However, variations of the temperature within a reasonable range have a negligible effect; thus, the Fermi functions can effectively be replaced by step functions. The values of γ providing adequate deconvolution (i.e. artefact-free, positive DOS) depend on the data sampling; they were determined empirically and found to fall in the 0.5%-2% range. The value of $\Delta = 152 \pm 5\,\mu$eV was determined to provide best overall consistency and is compatible with the estimated gap of our Ti/Al bilayer.

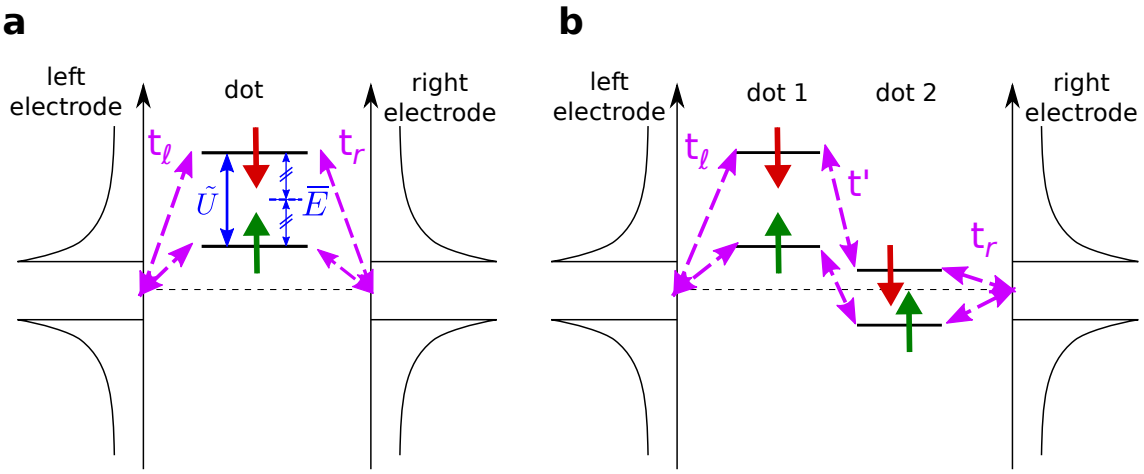

Figure 1: Schematic representation of the models used for describing the experimental data using a single (left panel) our a double (right panel) Quantum Dot model. See text for a more detailed explanation.

Spectral density for a double-quantum dot model connected to superconducting leads

Like in many experiments on nanotubes, our model is directly based on the standard quantum dot picture: The dot is seen as a series of electronic orbitals with different configuration energy that can each accommodate two electrons, and the Coulomb interaction between electrons is taken into account by a charging energy for each added electron. Even when this system is a many-body problem which cannot be solved exactly when the coupling to the leads is finite, it is possible to have a fairly good representation of its spectral properties using an effective non-interacting model. We shall first discuss how this effective model arises from a more general interacting Hamiltonian and then derive the DOS within this simple framework.

We start with a model of the nanotube as a double Quantum Dot (QD) connected to superconducting leads, restricting to a single orbital per dot, but with interactions and arbitrary couplings. Note that this model with a single dot (Fig. S1a, corresponding to the Anderson impurity model) would be sufficient to have ABS, but we have found necessary to consider a double dot structure to capture all the features observed in the data. The model is schematically depicted in Fig. S1b and the corresponding Hamiltonian can be written as $\hat{H} = \hat{H}_d + \hat{H}_T + \hat{H}_L + \hat{H}_R$, where

$$\hat{H}_d = \sum_{\alpha,\sigma} \epsilon_\alpha d^\dagger_{\alpha\sigma} d_{\alpha\sigma} + \sum_\alpha U_\alpha n_{\alpha\uparrow} n_{\alpha\downarrow} + \sum_\sigma t' d^\dagger_{1\sigma} d_{2\sigma} + \text{h.c.},$$

describe the electronic states and their Coulomb interactions in the central region. Here $d^\dagger_{\alpha\sigma}$ creates an electron in dot $\alpha = 1, 2$ with spin $\sigma = \uparrow, \downarrow$ and $n_{\alpha\sigma} = d^\dagger_{\alpha\sigma} d_{\alpha\sigma}$. The interactions are reduced to the local charging energies U_α on each dot. For the sake of simplicity we neglect the interdot Coulomb interaction which was found to be negligible in experiments on double QD systems based on CNTs [4]. The term in t' corresponds to the interdot tunneling.

On the other hand the leads are described as ideal conductors accomodating one spin-degenerate channel with BCS pairing:

$$H_j = \sum_{\boldsymbol{k}\sigma} \xi_{\boldsymbol{k}} c^\dagger_{j\boldsymbol{k}\sigma} c_{j\boldsymbol{k}\sigma} + \sum_{\boldsymbol{k}} \left(\Delta e^{i\varphi_j} c^\dagger_{j\boldsymbol{k}\uparrow} c^\dagger_{j,-\boldsymbol{k},\downarrow} + \text{h.c.} \right),$$

where $c^\dagger_{j\boldsymbol{k},\sigma}$ creates an electron with wavevector$\boldsymbol{k}$ in lead $j = L/R$, $\xi_{\boldsymbol{k}}$ and Δ are the single-particle energy and the gap parameter respectively (assumed to be equal for $j = L/R$) while in the main text $\varphi = \varphi_L - \varphi_R$ denotes the superconducting phase difference between the leads. The leads are also characterized by a normal density of states ρ_n. Finally, the spin-conserving tunneling Hamiltonian can be written as $H_T = \sum_{j\boldsymbol{k}\sigma} t_j c^\dagger_{j\boldsymbol{k}\sigma} d_{\alpha_j\sigma} + \text{h.c.}$, where $\alpha_j = 1(2)$ for $j = L(R)$ and t_j denote the hopping elements $t_{\ell,r}$ illustrated in the right panel of Fig. S1. For simplicity we take t_j and t' to be real quantities.

Finding the spectral properties of this model in the general case, including the effects of electron correlations, is a formidable task. For the case of the Anderson impurity model with superconducting leads several techniques have been applied, including Hartree-Fock approximation (HFA) [5], perturbation theory in U [6], Quantum Monte Carlo [7] and Numerical Renormalization Group (NRG) [8, 9]. In brief these works demonstrate that the system exhibits a magnetic S=1/2 ground state for $\Delta > k_B T_K$, where T_K is the Kondo temperature. In this regime the Andreev states spectrum predicted by the more sophisticated numerical techniques (NRG) [9] can be mimicked by a those of a simple non-interacting HFA [5] in which the level splitting between the two spin orientations is simply the charging energy times the difference in their population. We expect that other effects such as spin-orbit or exchange interactions (that the Anderson model cannot handle) could also modify the level splitting.

To describe in a simple way the behavior of the Andreev states spectrum in the different regimes, in the present work we thus adopt a phenomenological non-interacting approach (similar to HFA but) with effective parameters. For this, we replace H_d by $H_d^{eff} = \sum_{\alpha,\sigma} \tilde{\epsilon}_{\alpha\sigma} d^\dagger_{\alpha\sigma} d_{\alpha\sigma} + \sum_\sigma t' d^\dagger_{1\sigma} d_{2\sigma}$ + h.c., where $\tilde{\epsilon}_{\alpha\downarrow} = \tilde{\epsilon}_{\alpha\uparrow} + \tilde{U}_\alpha$. In this way the model describes both the case of nearly degenerate spin states (for $\tilde{U}_\alpha \ll \Delta$) and well resolved spin states (for $\tilde{U}_\alpha \gg \Delta$). The effective charging energy $\tilde{U}_\alpha$ is then a parameter which has to be determined by fitting the experiment. Notice that the ordering of the spin states implied by $\tilde{\epsilon}_{\alpha\downarrow} = \tilde{\epsilon}_{\alpha\uparrow} + \tilde{U}_\alpha$ is conventional. We cannot tell which spin direction is populated first in a given dot but once a spin orientation is selected for the first electron, the second electron should have the opposite. It should be emphasized that spin symmetry is not broken on average.

We can then obtain the spectral properties of this model from the retarded Green function in the orbital-Nambu space defined as $\hat{G}_\sigma(t,t') = -i\theta(t,t') < \left[\psi_\sigma(t), \psi^\dagger_\sigma(t')\right]_+ >$, where $\psi_\sigma = (d_{1,\sigma}, d_{2,\sigma}, d^\dagger_{1,-\sigma}, d^\dagger_{2,-\sigma})$. In the frequency representation this quantity adopts the form $\hat{G}_\sigma(\omega) = \left[\omega - \hat{h}_\sigma - \hat{\Sigma}(\omega)\right]^{-1}$, where

$$\hat{h}_\sigma = \begin{pmatrix} \tilde{\epsilon}_{1,\sigma} & t' & 0 & 0 \\ t' & \tilde{\epsilon}_{2,\sigma} & 0 & 0 \\ 0 & 0 & -\tilde{\epsilon}_{1,-\sigma} & -t' \\ 0 & 0 & -t' & -\tilde{\epsilon}_{2,-\sigma} \end{pmatrix}$$

and

$$\hat{\Sigma}(\omega) = \begin{pmatrix} \Sigma_1^{ee} & 0 & \Sigma_1^{eh} & 0 \\ 0 & \Sigma_2^{ee} & 0 & \Sigma_2^{eh} \\ \Sigma_1^{he} & 0 & \Sigma_1^{hh} & 0 \\ 0 & \Sigma_2^{he} & 0 & \Sigma_2^{hh} \end{pmatrix},$$

with $\Sigma^{ee}_{\alpha_j} = \Sigma^{hh}_{\alpha_j} = \Gamma_j g(\omega)$ and $\Sigma^{eh,he}_{\alpha_j} = -\Gamma_j e^{\pm i\varphi_j} f(\omega)$. In these expressions $f(\omega) = \Delta/\sqrt{\Delta^2 - (\omega + i\eta)^2}$ and $g(\omega) = -(\omega + i\eta) f(\omega)/\Delta$ are the dimensionless BCS green functions of the uncoupled leads (where we have included a finite inelastic relaxation rate η as a phenomenological parameter) and $\Gamma_j = \pi \rho_n t_j^2$ are the so-called normal tunneling rates to the leads. Obtaining $\hat{G}_\sigma(\omega)$ thus corresponds to the inversion of a 4×4 matrix which we perform numerically. From this quantity one can directly express the spectral densities as

$$\rho_{\alpha\sigma}(\omega) = -\frac{1}{\pi} \mathrm{Im}\left[\hat{G}_\sigma(\omega)\right]_{\alpha,\alpha}.$$

Note that in the fits of the differential conductance we allow for different tunneling rates, Γ^p_α between the probe electrode and the two sides of the double-QD. This is justified by the broken symmetry which is expected between the two quantum dots. Figures 3c and 4 thus show the quantity $\sum_{\alpha,\sigma} \Gamma^p_\alpha \rho_{\alpha\sigma}(\omega)$. We do not fit the total intensity but rather fix the relative visibility Γ^p_1/Γ^p_2 (the complete list of parameters for the fits of Figs. 3c and 4 is given below).

Parameters used for the theoretical figures

The parameters used in figure 3c of the article are:

group	1		2				3		4				5		6		7			
V_n^0(V)	-10.12	-10.08	-10.33	-9.84	-9.49	-9.25	-9.045	-8.807	-8.08	-7.95	-7.84	-7.43	-6.739	-6.408	-6.65	-6.65	-6.00	-5.77	-5.48	-5.19
spin	↑	↓	↑	↓	↑	↓	↑	↓	↑	↓	↑	↓	↑	↓	↑	↓	↑	↓	↑	↓
$\Gamma_{\ell,r}/\Delta$	0.90		0.81		1.21		1.0		0.81		1.96		1.21		2.10		0.75		2.40	
t'/Δ	-		1.25				-		0.8				-		-		1.1			
visibility	0.5		1		0.5		1		1		0.5		1		0.5		1		0.5	

and those in figure 4 of the article are:

group	1			
V_n^0(V)	-11.65	-11.53	-11.382	-11.085
spin	↑	↓	↑	↓
$\Gamma_{\ell,r}/\Delta$	2.10		1.11	
t'/Δ	1.0			
visibility	0.5		1	

In these tables, V_n^0 is the gate voltage at which the given level crosses the Fermi level. The spin orientation shown here only indicate the relative spin orientation within a given group. We have assumed that all levels have identical capacitances to the gate. Their respective energies as a function of the gate voltage are thus given by $\epsilon_n(V_g) = \lambda\Delta \times (V_g - V_n^0)$, with a value of $\lambda = +12\,V^{-1}$ determined in data where the Coulomb diamonds are most visible. For groups of levels involving two SSPL, one of them is coupled to the left lead with Γ_ℓ, the other one to the right lead with Γ_r, and they are coupled together with a hopping term t', as show on the right panel of Figure S1. For single SSPLs $\Gamma_{\ell,r}$ denotes either the left or right coupling. The visibility gives the relative weight of a pair of levels in the measurement of

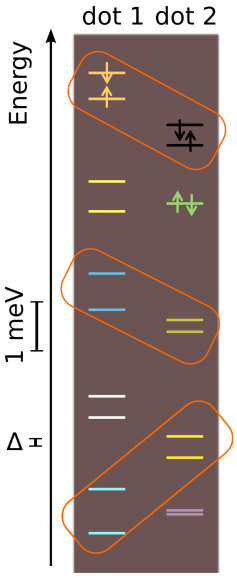

Figure 2: Possible arrangement of the levels of Fig. 3c in the two dots. In this picture, each color corresponds to a pair of levels extracted from the ABS spectroscopy and given in the table (we use the same colors as the lines in Fig3c). The various orbitals were assigned to either dot to yield the most uniform level spacing in each dot, which is of course an "aesthetic" and arbitrary assumption we cast on the system. The boxes represent the pairs of levels for which we needed to take into account inter-dot coupling, to reproduce avoided crossing. In each pair the electrons are of opposite spin, but there is no preferred overall orientation. Hence, the arrows shown here only indicate the relative spin orientation of the levels, as obtained from ABS spectroscopy.

the DOS by the tunnel probe (see previous section).

From these parameters we can give a tentative picture of the ladder of levels in the two dots, as shown in Fig S2. Such a level representation is easier to apprehend than the set of apparently random lines shown in Fig 3c.

Quantum dot vs. Fabry-Pérot description

We also measured a device, shown in Figure S3, which was better coupled to the leads than the sample analyzed in the main text (for which we had coupling Γ in the range $0.8-2.4\times\Delta$). The DOS at energies $|E|\geq\Delta$ (the continuum) shows weak modulations with the gate voltage rather than sharp features. These modulations can arise in two different regimes.

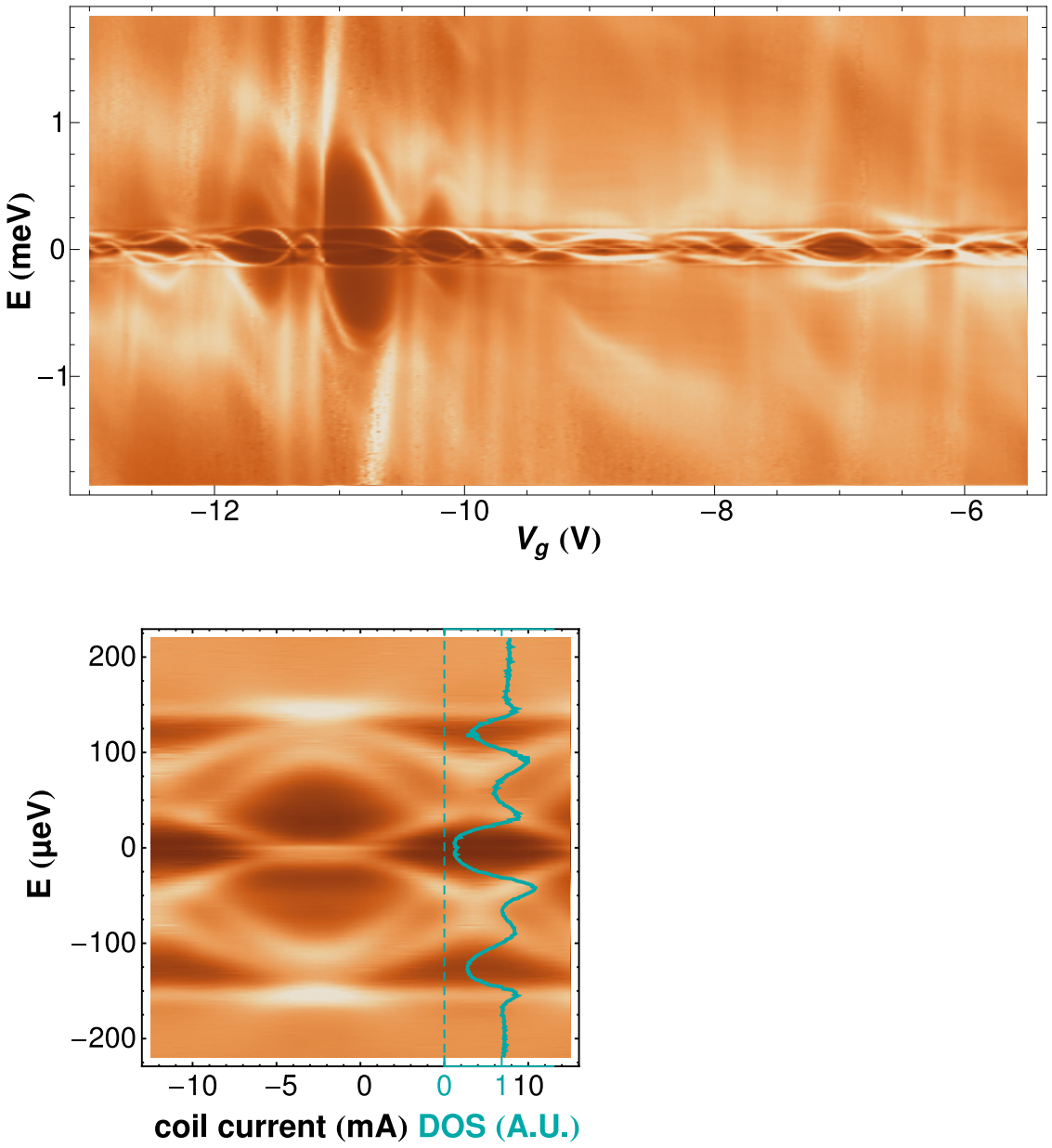

Figure 3: Top panel : Deconvolved DOS data from a different device than the one shown in the main text. We see almost everywhere more ABS in the gap, each extending on larger V_g range and overlapping with others. This indicates that the nanotube in this device was better coupled to the leads than the one in the main article. Bottom panel: flux dependence at $V_g = -6.02V$.

In the first regime, the nanotube is characterized by a continuum of states (this would be true for nanotube devices in which finite-size effects are negligible). In this situation the weak modulations of the DOS at energies above the gap are generated by Fabry-Perot

interference due to weak backscattering at the two contacts. Moreover, for energies below the gap, this model predicts continuous bands of ABSs.

The second situation that can give rise to weak modulations of the DOS above the gap is that of a nanotube exhibiting discrete levels that are well separated in energy (i.e. a short nanotube behaving as a quantum dot), but also well coupled to the leads. This is the model discussed in the previous two sections. Above the gap, this model shows that the good coupling with the leads gives rise to weak modulations of the DOS: the stronger the coupling, the smoother the fluctuations in the DOS. However, inside the gap, one should see discrete Andreev levels that are not broadened by the coupling with the leads. Nevertheless, the good coupling makes the variation of the ABS energies with the gate voltage slower than in the weak coupling situation, thus the observed ABS remain within the gap for larger intervals of gate voltages and, consequently, a larger number of ABS resonances are observed at a given gate voltage.

Thus we see that, while two possible models for the nanotube can give rise to the same type of features in the spectroscopic features above the gap, inside the gap the two models give rise to very distinct features, as long as one can resolve discrete ABS. In particular, since our experimental data shows distinct ABS inside the gap, it suggests that the studied nanotube behaves as a discrete quantum dot rather than as a plain continuum of states. On the other hand, a continuum model properly including all the effects of backscattering should also be able to account for the observed features.

Our results indicate that for nanotube devices with good coupling to the leads, quantum dot models may be more broadly applicable than previously thought. This also underlines that in efforts to reveal Luttinger Liquid physics in nanotube devices, it is important to take finite-size effects and in particular discrete energy spectra into account.

Width of the resonances - Lifetime of the ABS

The analysis of the ABS linewidth in the deconvolved DOS gives a FWHM of 30-40 µeV, independent of gate voltage and flux. If this linewidth is intrinsic, it would correspond to a sub-ns coherence time of the ABS. Possible extrinsic sources for this linewidth are

- Charge or flux noise. These cannot be the dominant contribution to the linewidth since the latter is essentially independant of the flux and of the gate voltage.

- The tunneling current from the probe. The electron tunneling rate from the probe limits the lifetime of the ABS. This rate can be exactly evaluated by integrating the differential current measurements. This mechanism would give a linewidth of less than 1 μeV for all peaks shown.

- Non thermal-equilibrium voltage noise on the tunnel probe. This would smear out the measured peaks and it would also dephase the ABS by the capacitive action of the probe. The level of noise necessary to explain the observations would be somewhat higher than what was measured ($\sim 15\,\mu$eV) previously in a very closely related setup [1]. This cannot be ruled out at present, however.

- Finally, a finite residual density of states in the superconducting gap could also yield this linewidth. This can easily be included in the theory by the introduction of a Dynes depairing parameter [2], and it is exactly what we have done to produce the theoretical predictions of the DOS from the Green functions. This turns out to produce ABS linewidth independent of gate voltage and flux. The observed linewidth is qualitatively reproduced for a Dynes depairing parameter of $\sim 10 - 15\%$ of Δ. Unfortunately we could not check directly in this setup the density of states of the superconducting electrodes, and moreover, it is difficult to distinguish such a depairing effect from that of voltage noise [10]. Repeating such an experiment with different superconducting materials could shed some light on this issue.

For the time being, the simplest candidate explanation for the measured linewidth is the presence of uncontrolled noise in the measurement. Further investigation is clearly needed to precisely establish the origin of the measured linewidth and assess the potential of ABS as qubits.

---

[1] le Sueur, H., Joyez, P., Pothier, H., Urbina, C. & Esteve, D. Phase controlled superconducting proximity effect probed by tunneling spectroscopy. *Physical Review Letters* **100**, 197002 (2008).

[2] Dynes, R. C., Narayanamurti, V. & Garno, J. P. Direct measurement of Quasiparticle-Lifetime broadening in a Strong-Coupled superconductor. *Physical Review Letters* **41**, 1509 (1978).

[3] Wikipedia. Moore–Penrose pseudoinverse. http://en.wikipedia.org/wiki/Moore-Penrose_pseudoinverse (2010).

[4] Gräber, M. R. *et al.* Molecular states in carbon nanotube double quantum dots. *Physical Review B* **74**, 075427 (2006).

[5] Rozhkov, A. V. & Arovas, D. P. Josephson coupling through a magnetic impurity. *Physical Review Letters* **82**, 2788 (1999).

[6] Vecino, E., Martín-Rodero, A. & Levy Yeyati, A. Josephson current through a correlated quantum level: Andreev states and pi junction behavior. *Physical Review B* **68**, 035105 (2003).

[7] Siano, F. & Egger, R. Josephson current through a nanoscale magnetic quantum dot. *Physical Review Letters* **93**, 047002 (2004).

[8] Tanaka, Y., Oguri, A. & Hewson, A. C. Kondo effect in asymmetric Josephson couplings through a quantum dot. *New Journal of Physics* **9**, 115–115 (2007).

[9] Lim, J. S. & Choi, M. Andreev bound states in the Kondo quantum dots coupled to superconducting leads. *Journal of Physics: Condensed Matter* **20**, 415225 (2008).

[10] Pekola, J. P. *et al.* Photon assisted tunneling as an origin of the dynes density of states. *1001.3853* (2010).